ChemComm

RSC Publishing

COMMUNICATION

View Article Online
View Journal | View Issue

Cite this: *Chem. Commun.*, 2013, **49**, 3025

Received 30th January 2013,
Accepted 26th February 2013

DOI: 10.1039/c3cc40788h

www.rsc.org/chemcomm

Hierarchical nanostructures with unique Y-shaped interconnection networks in manganese substituted cobalt oxides: the enhancement effect on electrochemical sensing performance†

Wen-Jie Lan, Cheng-Chi Kuo and Chun-Hu Chen*

A general redox procedure was successfully developed for the controlled synthesis of substituted cobalt oxides with hierarchical flower-like nanostructures comprising unique Y-shaped interconnections. The substitution and nanostructures synergistically enhance the material's electrochemical activities for highly efficient sensing of H_2O_2.

Controlled synthesis of complex nanostructures for achieving specific compositions, morphologies, and phases provides the unique opportunities to manipulate a material's properties and performances for specific applications.[1] However, achieving all these control requirements in one synthetic procedure is challenging, and even more difficult for multi-component materials. Redox reaction is generally a stoichiometric process because the number of electrons transferred in a particular reaction is highly restricted. This characteristic leads to the potential to control elemental ratios in multi-component products. With a proper design of the redox reagents, the desired substitutes can be delivered into the host materials *via* the redox reactions to accomplish specific compositions, phases, and even nanostructures simultaneously in one step. Nevertheless, systematic studies of this concept for the controlled synthesis of multi-component nanomaterials are rarely reported.

Cobalt oxides are versatile materials for emerging fields, such as clean energy, biomaterials, and catalysis.[2] Nanostructured cobalt oxide hydroxide (CoOOH) and Co_3O_4 materials have remarkable electrochemical properties for applications in batteries, fuel cells, sensors, and others.[3,4] For many of these applications, high surface area and conductivities of materials are essential. Structural substitution is known as an effective approach to enhance the conductivities and add more functionalities to the materials, particularly with the mixed-valence species (*e.g.* MnO_x, CrO_x, *etc.*). In addition, structural substitution could assist in the formation of high surface area features to facilitate the interfacial electrochemical reactions. For the production of highly efficient cobalt oxides, novel and general approaches for structural substitution and high surface area nanostructures are highly desired.

In this work, general redox procedures utilizing metal-containing oxidants (*e.g.* MnO_4^- and CrO_4^{-2}) for the controlled synthesis of substituted cobalt oxide materials are demonstrated. The redox reactions between Co^{2+} and metal-containing oxidants were designed for the occurrence of structural substitution with a narrow range of composition variation, as well as the formation of porous three dimensional flower-like nanostructures. The results show that this concept could be general for developing novel substituted metal oxide nanomaterials with highly efficient electrocatalytic activities.

The nanostructured cobalt manganese oxide hydroxide (CMOH) materials were prepared first *via* the one-pot reactions of cobalt sulfate and potassium permanganate at 100 °C for 24-hour. The XRD results of CMOH are shown in Fig. 1a, exhibiting a single phase corresponding to the CoOOH structure (JCPDS-07-169). The scanning electron microscopy (SEM) images of CMOH show the 3D flower-like nanostructures with three levels of hierarchical structures (Fig. 2a). The primary structure is referenced to the layered crystal structure of the CoOOH phase. The secondary structure is the 3D flower-like nanoscale features with the thickness of the nanoflakes being 5–10 nm (Fig. 2a). The spherical morphology with diameters around 0.5–1 um is defined as the tertiary structure. In the high magnification SEM images (Fig. 2b), the unique Y-shaped subunits of the secondary structure are revealed, and labelled by the green Y mark in Fig. 2c. The multiple and complex interconnections between these Y-shaped subunits, as demonstrated by the interconnection of

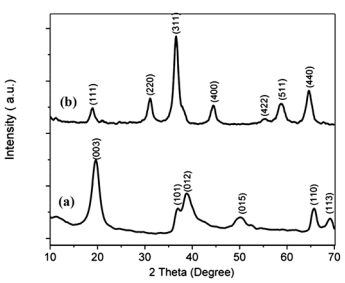

Fig. 1 The XRD patterns of the as-obtained cobalt manganese oxide hydroxide (CMOH) (a), and the spinel cobalt manganese oxide (CMO) after the calcination (b).

Department of Chemistry, Center for Nanoscience and Nanotechnology, National Sun Yat-sen University, Kaohsiung, Taiwan 80424.
E-mail: chunhu.chen@mail.nsysu.edu.tw

† Electronic supplementary information (ESI) available: Synthetic procedure and characterization results, and Fig. S-1–S-7. See DOI: 10.1039/c3cc40788h

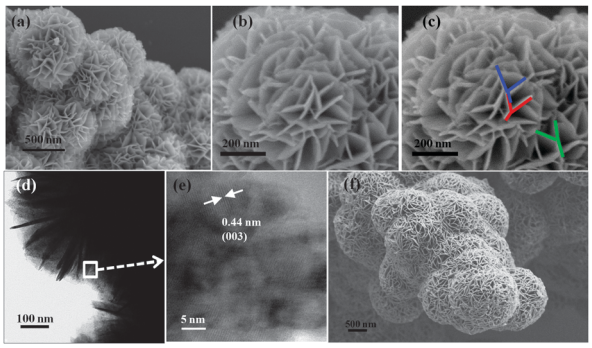

Fig. 2 The electron microscopy images of manganese substituted cobalt oxides: (a) the SEM images of CMOH; (b) the higher magnification images of the secondary structure in CMOH materials; (c) the marks of Y-shaped interconnections corresponding to the image in (b); (d) TEM images of CMOH; (e) the HR-TEM images corresponding to the white square area in (b); (f) the SEM images of CMO obtained after the calcination of CMOH.

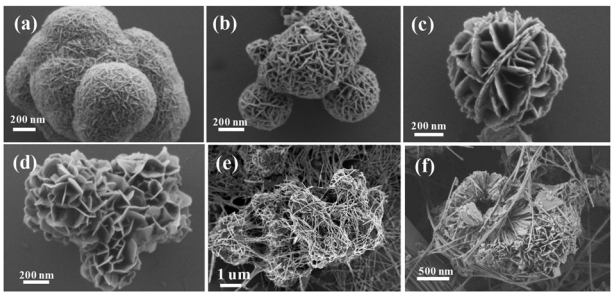

Fig. 3 The morphological evolution of CMOH with various reaction temperatures: (a) 60 °C, (b) 80 °C, (c) 120 °C, (d) 150 °C, and (e)–(f) for 200 °C.

the blue and red Y marks, result in the networks of flower-like nanostructures. Such Y-shaped secondary structures have not been clearly identified in substituted cobalt oxide systems. The continuous networks of the Y-shaped interconnections lead to the dense microspherical tertiary structure without hollow cores, as confirmed by the TEM images (Fig. 2d). The high resolution TEM images show a 0.44 nm spacing of the lattice fringes in CMOH (Fig. 2e), corresponding to the interlayer d_{003} in the CoOOH structure as the primary structure. No additional phases/impurities of cobalt or manganese oxides were observed in the XRD, SEM, and TEM results. The elemental analyses using EDXS show the presence of cobalt and manganese with a homogeneous distribution in CMOH (Fig. S-1, see ESI†), indicating the success of manganese substitution *via* metal-containing oxidants. The appearance of unique Y-shaped interconnections is different from the isolated, flat, and hexagonal-shaped particles of pure CoOOH materials with metal-free oxidants (*e.g.* ClO^-, H_2O_2, NO_2^-, *etc.*) reported in the literature,[5] clearly showing that manganese substitution alters the growth mechanism of the materials.

To understand the possible growth process of the flower-like nanomaterials in CMOH, a series of time- and temperature-dependent experiments were conducted. The results of time-dependent experiments (Fig. S-2, ESI†) show that the spherical aggregations with the diameters of 100–150 nm were rapidly generated after a 0.5 hour reaction, but flower-like nanostructures or Y-shaped interconnections were not clearly observed. The samples obtained after a one hour reaction exhibit the porous nanostructures on the surface with the average particle diameter around 300 nm. With the further proceeding of reactions to two-hours, the Y-shaped subunits and flower-like nanostructures were observed with enlarged diameters. After the extension of the reaction time to 4 and 8 hours, the development of flower-like structures was complete with a continuous growth of the tertiary structure. The XRD results (Fig. S-3, ESI†) suggest that the CoOOH phase was formed right after the 0.5 hour reaction. The temperature-dependent experiments show that the growth of flower-like nanostructures is sensitive to the reaction temperatures (Fig. 3). The origin (or seeds) of Y-shaped subunits was observed at 60 °C. Within the temperature range of 80–150 °C, the higher reaction temperatures assist the growth of the volume of nanoflakes with the internal spacing expansion between each Y-shaped interconnection. At the elevated temperatures, complex and highly porous secondary structures can be fully resolved by the Y-shaped features. At 200 °C, the presence of impure phases/materials is observed from two different morphologies, nanowires (Fig. 3e) and microspheres (Fig. 3f), and inhomogeneous elemental distribution (Fig. S-4, ESI†), showing the synthetic limits of CMOH due to impurity formation.

The CoOOH-structure materials are versatile precursors to obtain functional cobalt oxide derivatives. Nevertheless, the thermal stability issues of the Y-shaped secondary structure, such as phase separation/re-precipitation particularly for binary metal oxides, need to be considered if additional thermal treatments are required for the phase transformation. After a thermal treatment of CMOH at 500 °C for 6 hours, the XRD patterns show that the CoOOH structure can be transformed to a cubic spinel Co_3O_4 structure without the presence of impure phases (Fig. 1b). The SEM images of these spinel cobalt manganese oxide (CMO) materials show no significant changes in the Y-shaped networks/flower-like nanostructures (Fig. 2f), demonstrating the promising stability of the secondary structures in binary CMOH as the general precursors for various substituted cobalt oxide materials. This is particularly important for many binary materials that cannot be directly prepared with the Y-shaped nanoscale networks if 3D nanostructures are desired. The specific surface areas of CMO and CMOH are summarized in Table S-1 (ESI†). After the calcination, an increase in surface area is observed in CMO samples. The increased percentages (~40%) are very similar between the CMO samples with different cobalt-to-manganese ratios, suggesting that certain phase transformation mechanisms coupled with the new surface exposure processes could be involved.

The CMO materials with highly porous Y-shaped features and structural substitution are superior candidates for electrochemical sensing applications. The detection of hydrogen peroxide provides valuable biological signals regarding enzymatic reactions catalyzed by various oxidases, such as glucose oxidase and peroxidase.[4d,6] Thus enzyme-free sensing of H_2O_2 reduction was selected as the model reaction to test the electrochemical activities of CMO materials. The cyclic voltammetry (CV) results in Fig. 4a show that the CMO modified electrodes exhibit greatly enhanced H_2O_2 reduction currents than those of commercial Co_3O_4, demonstrating the strong electrochemical activities of CMO for H_2O_2 reduction. The effect of the Y-shaped secondary

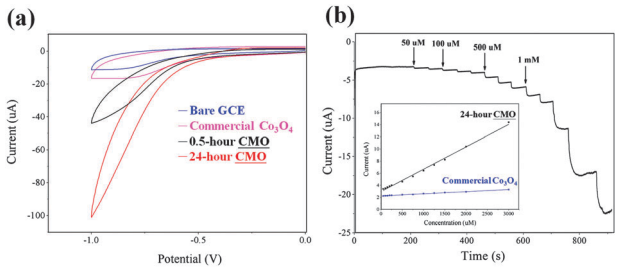

Fig. 4 The electrochemical studies of CMO materials for H_2O_2 sensing. (a) The cyclic voltammograms of various electrodes in the phosphate buffer solution (PBS) with 1 mM H_2O_2; (b) the amperometric response of 24-hour CMO electrodes with the successive injection of H_2O_2 to 0.1 M PBS at an applied potential of −0.6 V; the inset presents the comparison of calibration curves of 24-hour CMO (black line) and commercial Co_3O_4 (blue line).

structure on electrochemical performance is investigated through the activity comparison of CMO prepared with different reaction times (0.5 and 24-hour, Fig. S-2, ESI†). The 24-hour CMO samples with the matured flower-like nanostructures show much higher currents than the 0.5-hour CMO samples, demonstrating the enhancement role of the 3D flower-like nanostructures.

The amperometric responses of the 24-hour CMO modified electrodes show rapid and sensitive signals to the changes in H_2O_2 concentrations (Fig. 4b). The comparison of the calibration curves between the 24-hour CMO and commercial Co_3O_4 shows that the sensitivities of 24-hour CMO are around 9 times greater than that of the commercial Co_3O_4. The presence of porous Y-shaped interconnections contributes to the 2.6-times increase in sensitivity observed from the comparison of 0.5-hour and 24-hour CMO (Fig. 3b and S-5, ESI†). These results explicitly show the important impacts of hierarchical nanostructures and substitution on superior electrochemical activities.

Several CMOH materials prepared with different substitution levels of Mn were conducted (Co/Mn from 3 to 10) to further understand the formation pathway. The elemental analysis results show that only a small decrease in Mn contents was measured in these CMOH products even with the dramatic drops in the Mn^{7+} amount used in the preparation procedure (Table S-2, ESI†), giving a good control of elemental compositions compared with other doping approaches. In addition, no products can be generated in the absence of Mn^{7+} under the same synthetic conditions. These results together indicate the dual roles of metal-containing oxidants: redox reagents and substitute delivery. The redox reaction between Co^{2+} and Mn^{7+} results in the small variation of Co/Mn ratios in the products due to the specific electron transfer process. In the lowest Mn content tests (Co/Mn = 10), the Co/Mn ratios of the products are very close to 3. The XPS results also confirm the presence of Co^{3+} and Mn^{4+} in the CMOH (Fig. S-6, ESI†), suggesting the following redox relationship:

$$3Co^{2+} + Mn^{7+} \rightarrow 3Co^{3+} + Mn^{4+} \quad (1)$$

To preliminarily verify the generality of the structural substitution concept *via* metal-containing oxidants, another redox example of Co^{2+} and Cr^{6+} was carried out. The formation of nanostructured microspheres with assembly of flake-like particles was successfully obtained with the CoOOH structure (Fig S-7, ESI†). The EDXS results also confirm the structural substitution of chromium. The absence of Y-shaped interconnections indicates that the formation of unique nanostructures is dependent on the substitute species. The generality and effectiveness of the redox routes utilizing metal-containing oxidants for diverse binary metal oxide nanomaterials is demonstrated.

In summary, we first reported the unique hierarchical nanostructures with Y-shaped interconnections in highly active Mn substituted cobalt oxide materials, and demonstrated the proof-of-concept utilizing a redox process to perform composition-specific structural substitution. The control of the hierarchical nanostructures/Y-shaped features can be achieved *via* selection of certain reaction time and temperatures. The high surface area nanostructures and Mn substitution result in CMO materials with superior electrochemical activities for H_2O_2 biosensor applications. Diverse nanostructures are awaiting to be explored with different substitute species. Further development of various substituted metal oxide systems for sensors, catalysis, and clean energy applications is being actively pursued.

We acknowledge the support of the Taiwan National Science Council under Grant NSC101-2113-M-110-005-MY2. We also thank Professor Chao-Ming Chiang and Chi-Wi Ong for valuable discussion.

Notes and references

1 (*a*) Y. D. Yin, R. M. Rioux, C. K. Erdonmez, S. Hughes, G. A. Somorjai and A. P. Alivisatos, *Science*, 2004, **304**, 711–714; (*b*) M. H. Huang and P.-H. Lin, *Adv. Funct. Mater.*, 2012, **22**, 14–24; (*c*) K. Zhou and Y. Li, *Angew. Chem., Int. Ed.*, 2012, **51**, 602–613; (*d*) Y. Li, W. Cai, B. Cao, G. Duan, F. Sun, C. Li and L. Jia, *Nanotechnology*, 2006, **17**, 238–243; (*e*) Y. Li, N. Koshizaki, H. Wang and Y. Shimizu, *ACS Nano*, 2011, **5**, 9403–9412; (*f*) Y. Li, C. Li, S. O. Cho, G. Duan and W. Cai, *Langmuir*, 2007, **23**, 9802–9807; (*g*) P. Yang, X. Xiao, Y. Li, Y. Ding, P. Qiang, X. Tan, W. Mai, Z. Lin, W. Wu, T. Li, H. Jin, P. Liu, J. Zhou, C. P. Wong and Z. L. Wang, *ACS Nano*, 2013, DOI: 10.1021/nn306044d.

2 (*a*) Y. Liang, Y. Li, H. Wang, J. Zhou, J. Wang, T. Regier and H. Dai, *Nat. Mater.*, 2011, **10**, 780–786; (*b*) X. W. Xie, Y. Li, Z. Q. Liu, M. Haruta and W. J. Shen, *Nature*, 2009, **458**, 746–749; (*c*) Y. Ding, Y. Wang, L. Su, M. Bellagamba, H. Zhang and Y. Lei, *Biosens. Bioelectron.*, 2010, **26**, 542–548.

3 (*a*) H. Zheng, F. Tang, M. Lim, T. Rufford, A. Mukherji, L. Wang and G. Lu, *J. Power Sources*, 2009, **193**, 930–934; (*b*) V. Pralong, A. Delahaye-Vidal, B. Beaudoin, J.-B. Leriche and J.-M. Tarascon, *J. Electrochem. Soc.*, 2000, **147**, 1306.

4 (*a*) F. Cheng and J. Chen, *Chem. Soc. Rev.*, 2012, **41**, 2172–2192; (*b*) F. Jiao and H. Frei, *Angew. Chem., Int. Ed.*, 2009, **48**, 1841–1844; (*c*) W. Y. Li, L. N. Xu and J. Chen, *Adv. Funct. Mater.*, 2005, **15**, 851–857; (*d*) M. S. Batista, R. K. S. Santos, E. M. Assaf, J. M. Assaf and E. A. Ticianelli, *J. Power Sources*, 2004, **134**, 27–32; (*e*) Y. Li, P. Hasin and Y. Wu, *Adv. Mater.*, 2010, **22**, 1926–1929.

5 (*a*) C.-H. Chen, S. F. Abbas, A. Morey, S. Sithambaram, L.-P. Xu, H. F. Garces, W. A. Hines and S. L. Suib, *Adv. Mater.*, 2008, **20**, 1205–1209; (*b*) B. Geng, F. Zhan, C. Fang and N. Yu, *J. Mater. Chem.*, 2008, **18**, 4977; (*c*) J. Yang, H. Liu, W. N. Martens and R. L. Frost, *J. Phys. Chem. C*, 2010, **114**, 111; (*d*) F. Bardé, M. R. Palacin, B. Beaudoin, A. Delahaye-Vidal and J. M. Tarascon, *Chem. Mater.*, 2004, **16**, 299–306.

6 (*a*) A. Salimi, R. Hallaj, S. Soltanian and H. Mamkhezri, *Anal. Chim. Acta*, 2007, **594**, 24–31; (*b*) J. Tian, H. Li, W. Lu, Y. Luo, L. Wang and X. Sun, *Analyst*, 2011, **136**, 1806–1809.